ORIGINAL PAPER

Modeling of ground motion rotational components for near-fault and far-fault earthquake according to soil type

Lila Kalani Sarokolayi · Ali Beitollahi ·
Gholamreza Abdollahzadeh ·
Seyed Taghi Rasouli Amreie · Saman Soleimani Kutanaei

Abstract The motion of a point is specified completely through six components, three translational and three rotational. Three rotational components of ground motion are classified to two rocking components and one torsional component. The transitional components of ground motion are easily measurable by standard techniques, whereas the rotational components are not directly accessible. In this study, the rotational component of production technique was described, and the influences of soil type and the distance from the fault on the rotational component were investigated. The results showed that the effect of the rotational components is more significant in low periods. Also, the value of the normalized response spectra for soft soil is more than stiff soil, but for far-fault earthquake, it is less than near-fault earthquake.

Keywords Rotational components · Normalized response spectrum · Near-fault and far-fault earthquake · Soil type

Introduction

Earthquake is one of the most destroying natural disasters (Chattopadhyay and Chattopadhyay 2009; Shahri et al.

L. K. Sarokolayi · S. T. R. Amreie
Department of Civil Engineering, Tabari University of Babol, Babol, Iran

A. Beitollahi · S. S. Kutanaei (✉)
Department of Engineering Seismology and Risk, Road, Housing and Urban Development Research Center (BHRC), Tehran, P.O. Box: 13145-1696, Iran
e-mail: samansoleimani16@yahoo.com

G. Abdollahzadeh
Department of Civil Engineering, Babol Noshirvani University of Technology, Babol, Iran

2011; Rafi et al. 2013; Deif et al. 2013). The seismic waves that spread out from the earthquake source to the entire Earth are usually measured at the ground surface by a seismometer which consists of three translational components. Translational components involve two horizontal in x and y axis and one vertical in z axis in Cartesian coordinate. However, a complete representation of the ground motion induced by earthquakes consists not only of those three components of translational motion but also three components of rotational motion plus six components of strain. Although theoretical seismologists have pointed out the potential benefits of measurements of rotational ground motion, they were not made until quite recently. Rotational movement was seen in 1958 for the first time in tombstones, big rocks, and upper parts of chimney attributed to earth motion rotational components (Gordon et al. 1970). Earth motion rotational components are not paid attention for two reasons: first, rotational components have small range, and seismographs were not able to register. Second, rotational motions effect were considered negligible (Bouchon and Aki 1982). Newmark (1969) was perhaps the first to establish a relationship between the torsional and translational components of a ground motion based on constant velocity of wave propagation assumption. Ashtiany and Singh (1986), with an idea close to Newmark (1969), tried to produce rotational components. Based on Newmark (1969) relations, other researchers such as Ghayamghamian et al. (2009) using data collected from the Chiba dense array generated the torsional ground motion and analyzed several building models for different structural characteristics subjected to six correlated components of earthquake. Gomberg (1997) estimated the rotational components induced in the Northridge, California earthquake using classical relationships and translational records. Relationships were derived by only considering S waves and estimating the apparent wave velocity. The apparent wave velocity was calculated using the arrival of the S wave and was used to

scale the velocity seismogram. Nouri et al. (2010) made a comparison between different methods of torsional ground motion evaluation.

Rotational components of the ground motion are not usually considered in seismic analysis and design of structures. Rocking ground motion is expected to influence the response of tall and slender structures and base-isolated structures (Wolf et al. 1983; Ashtiany and Singh 1986; Zembaty and Boffi 1994; Politopoulos 2010; Kalanisarokolayi et al. 2008, 2012). The effects of torsional ground motion are expected to be greatest in near-symmetric buildings (De La Llera and Chopra 1994). Hart et al. (1975) attributed the torsional response of most high-rise buildings during the 1971 San Fernando earthquake. Bycroft (1980) associated the differential longitudinal motion that he described as responsible for the collapse of bridges during the 1971 San Fernando earthquake and the 1978 Miyagi-Ken-Oki earthquake with rotational components of ground motion. Politopoulos (2010) identified the excitation of the rocking mode in a base-isolated building due to rocking excitations. Both studies were based on simplified assumptions including horizontally propagating waves in bedrock and vertically propagating shear waves.

Several instruments have been used to measure the rotational excitation. Some of these are a simple extension of the traditional inertial seismometer and are cost effective, whereas others invoke ideas from a completely different field and are expensive. Graizer (2009) reviewed the classical methods of measuring rotation. Using a GyroChip rotational sensor, Nigbor (1994) succeeded in recording rotational ground motions at a distance of 1 km from a large explosion at the Nevada Test Site (NTS). Using similar instruments, Takeo (1998, 2009) recorded rotational ground motions excited by nearby earthquakes offshore of the Izu Peninsula of Japan during an earthquake swarm in 1997 and in 1998, respectively. However, after Nigbor moved his equipment to a recording site in Borrego Mountain, Southern California, he did not record significant rotational ground motions, even with more than a decade of observations. The first application of a ring laser gyroscope as a rotational sensor applied in the field of seismology was reported by Stedman et al. (1995). Fully consistent rotational motions were recorded by a ring laser gyro installed at the fundamental station in Wettzell, Germany (Igel et al. 2005).

Lee and Liang (2008) have used Lee and Trifunac's (1985, 1987) method to develop theories and algorithms for generating rotational motion from the corresponding available translational motions. Some researchers (Li et al. 2004) proposed an improved approach to obtain the rotational components of a seismic ground motion which included the effect of the relative contributions of the P, SV, and SH waves to calculate time histories of rotational components. In the past decade, rotational motions generated by large earthquakes in the far field have been successfully measured at sites in Germany,

New Zealand, and Southern California (Igel 2007), and observations agree well with classical elasticity theory (Suryanto et al. 2006a, b). However, recent rotational measurements in the near field of earthquakes in Japan (Takeo 1998, 2009) and in Taiwan (Huang 2003; Liu et al. 2009) indicate that rotational ground motion are 10 to 100 times larger than expected from the classical theory.

Recently, site effects became an attractive topic for engineers (Abbaszadeh Shahri et al. 2011; Choobbasti et al. 2014; Janalizadeh et al. 2013; Tavakoli et al. 2014). Previous studies demonstrated that soft deposits fortify the ground's motion; therefore, the resulting devastations on these types of layers are more severe than the stiff layers (Rezaei et al. 2013; Kutanaei et al. 2011). It is proved that amplification phenomena occur frequently on the soft deposits (MirMohammad Hosseini and Asadollahi Pajouh 2012; Kutanaei et al. 2012). The main reason is the soft deposits include trapping of seismic waves which leads to difference impedance in the lower deposits or bedrock. Effects of alluvial deposits near the ground surface which amplify strong ground motions are called "site effects." Site amplification effects reduce with the increase of geometrical age. Also, an increase of bedrock depth has a considerable effect on site amplification effects (El-Hussain et al. 2013).

Previous studies show that rotational response by earth rotation is an important index of earthquake motion. In this paper, rotational components of ground motion are obtained using both classical elasticity and elastic wave propagation theories based on SV and SH wave incidence of the earthquake. The rotational component of production technique is described, and the influences of soil type and distance from the fault on the rotational component are investigated.

Earth motion rotational component production theoretical method

This serves as an input for theoretical and numerical methods with engineering application such as HAM and HPM (Soleimani et al. 2011, 2012; Taeibi-Rahni et al. 2011) and also several numerical methods with broad engineering applications such as finite difference and RBF-DQ methods (Jalaal et al. 2011; Bararnia et al. 2012; Ganji et al. 2009). Three main approaches have been developed to incorporate rotational motions in engineering applications: first, using analytical form; second, using components of translation motion; and third, direct registration of rotational components by optical dominant technology.

Analytical method

This method does not involve model and soil local feature that can be known as a defect of this method, but depending on the

source behavior, it can be used in the movement of the places close to the fault. Bouchon and Aki (1982) simulated a fallible slope with the relative displacement of 1 m analytically and calculated the strains of different points and the obtained rotational components of ground motion in various distances from the causative fault. The results showed a considerable decrease in peak rotation by increasing distance from fault. Castellani and Boffi (1989) confirmed the function of this method in the wave modeling with low frequency.

Rotational component production method from translational component

Considering theoretical relations, two general methods have been suggested to produce rotational component by translational components: (1) the extraction of rotational components through the equations of the classical elastic theory between translational motion in the board and rotation upstanding the board and (2) the extraction of rotational component based on the simultaneous use from the equations of the classical elastic and wave distribution theories. The first method was introduced by Newmark (1969), and its influence on the responses of the structure was investigated. Consequently, three methods were introduced to estimate rotational components based on translational components involving time derivation, finite difference, and geodetics.

Time derivation

Ashtiany and Singh (1986) achieved rotational components of ground motion on the basis of translational components. They stated that earthquake can produce both transverse and longitudinal waves. Longitudinal waves have no role in torsion production, but transverse waves can cause torsions in the structure using the mentioned method. They tried to produce rotational component translational accelerate register, in a point on ground surface.

$$\varphi_{gkk}(t) = \frac{1}{c_j} \cdot \frac{\partial}{\partial t} \left[\ddot{U}_{jj}(t) - \ddot{U}_{ii}(t) \right] \qquad (1)$$

where $\ddot{U}_{jj}(t)$ and $\ddot{U}_{ii}(t)$ are translational components of the accelerations in ii and jj directions, c_j is wave propagation velocity in jj direction, and $\varphi_{gkk}(t)$ is rotation round vertical direction on ii and jj directions.

Finite difference method

A dense array of seismic accelerometers provides a unique opportunity to characterize the spatial variability of ground motion in a small geographic region. In finite difference method, the average translational components between two

points ($\varphi_{gz}(t)$) are calculated based on their translational components.

$$\varphi_{gz}(t) = \frac{1}{2} \left[\frac{\ddot{U}_2(t) - \ddot{U}_1(t)}{\Delta y} - \frac{\ddot{\theta}_2(t) - \ddot{\theta}_1(t)}{\Delta x} \right] \qquad (2)$$

where $\ddot{U}_1(t), \ddot{U}_2(t), \ddot{\theta}_1(t)$ and $\ddot{\theta}_2(t)$ are translational acceleration at points 1 and 2 along y and x directions, respectively. Δx and Δy are the distance between two points, respectively. Chopra and Lallera (1994) investigated the effects of accidental torsion due to uncertainty in the in-plane stiffness of lateral load-resisting elements in one-story systems and rotational motion. They generate torsional components by measuring translational acceleration in the two points of a structure foundation. This method was also used by Hang (2003) to estimate translational components.

Geodetic method

The geodetic method (GM) (Spudich et al. 1995) can be considered as an extension of the work of Niazi (1986). The stations were distributed in a three-dimensional space, and the relative displacement between every two stations (with a common station called the reference station) was expressed as the displacement gradient matrix, with the assumption of being constant and the region of the array. After the stationary hypothesis and the identification of the strong-motion phase for every two stations, the spatial variability was then investigated by defining a normalizing parameter. This parameter was proportional to the separation distance and the ratio of the standard deviation of the torsional motion to the average standard deviation of the horizontal motions used in the calculation of torsional motion.

Direct registration of rotational components

Several instruments have been used to measure the rotational excitation such as laser gyroscope, tilt meter, solid state sensor, and geosensor. Graizer (2009) reviewed the classical method rotation measurement. Nigbor (1994) measured the rotational components of ground motion near a large explosion directly using commercial rotational velocity sensors in the aerospace field. This micro-electromechanical gyroscopic sensor was later deployed in the Borrego Valley in Southern California but did not record any earthquake rotational ground motion at the noise level of the sensor. Takeo (1998) suggested similar issues of sensor resolution to record the near-field rotational motion caused by small earthquakes using a similar aerospace sensor. Ring laser rotation sensors are the state-of-the-art technology for measuring rotational

excitation. These sensors work on the basis of principles of optical interferometry. Ring laser gyroscopes require sophisticated facilities; their operations are complex and are not compatible with large-scale permanent networks or mobile arrays (Stedman 1995).

Generation rotational components of earthquake

Rotational components due to body waves

Seismic ground motions are a direct result of plane harmonic waves arriving at the site close to the earthquake source. It is assumed that the direction of propagation of the waves lies in the vertical (x,z) plane. As the wave passes, it induces particle displacement in the perpendicular and parallel planes to the direction of propagation. The particle displacements in the plane which are perpendicular to the direction of propagation are decomposed into in-plane and out-of-plane components due to SV and SH waves, respectively. The parameters, A_S and A_0 depict amplitudes of in-plane and out-of-plane components, respectively. Incidence and reflection of the body waves will originate three rotational components of the ground motion at the free surface: φ_{gz}, φ_{gx}, and φ_{gy}. The component φ_{gz}, referred to as torsional component, is related to rotation about z axis, and the components φ_{gx} and φ_{gy}, referred to as the rocking components, are related to rotation about x axis and y axis, respectively.

Incidence SV wave

The coordinate system (x,z) and the incident and reflected rays associated with plane SV wave, reflecting off the free boundary of the elastic homogeneous and isotropic half space ($Z \leq 0$), are shown in Fig. 1a. Alongside preserving generality, it is assumed here that the incident and reflected rays are in the plane of $Y=0$. Amplitude of particle motion, u and w, along with the ray direction are presented by A_S, A_{SS}, and A_{SP}. It is assumed that the ray direction demonstrated positive displacement amplitudes. A_S, A_{SS}, and A_{SP} corresponded to incident SV wave, reflected SV wave, and reflected P wave, respectively. Considering this kind of excitation and coordination, the only definable non-zero components of motion located at $Y=0$ planes are:

The particles of displacement u, w in the x, z directions, respectively, are given by:

$$u = \frac{\partial \varphi_{sp}}{\partial x} + \frac{\partial(\psi_{SV} + \psi_{SS})}{\partial z} \tag{3}$$

$$u = \frac{\partial \varphi_{sp}}{\partial z} + \frac{\partial(\psi_{SV} + \psi_{SS})}{\partial x} \tag{4}$$

The relation between the rotational and translational motions in a point base on the classical elasticity theory can be expressed by:

$$\varphi_{gy} = \frac{1}{2}\left(\frac{\partial w}{\partial x} - \frac{\partial u}{\partial z}\right) \tag{5}$$

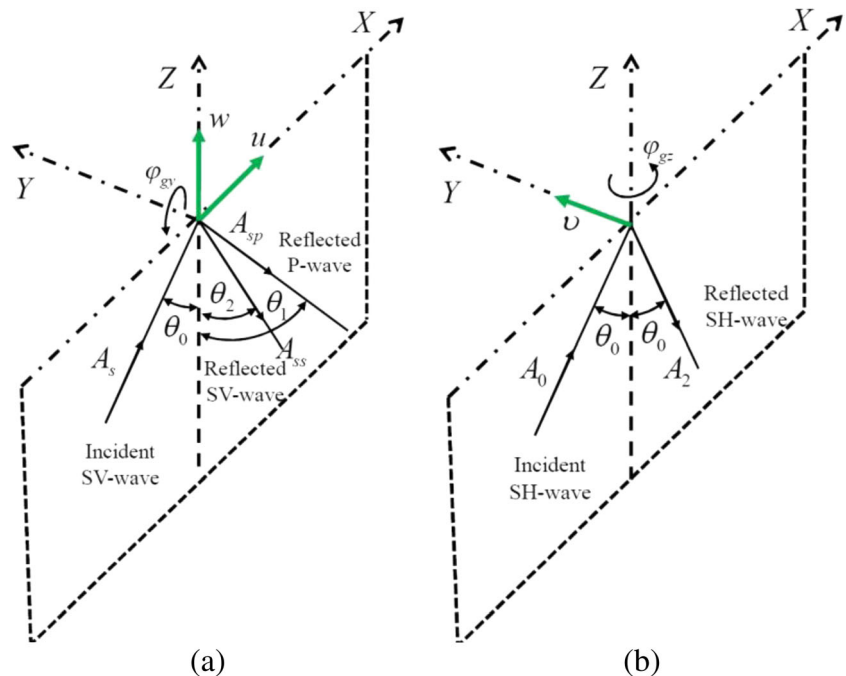**Fig. 1** Propagation of **a** incident SV wave and **b** incident SH wave

(a) (b)

Table 1 Characteristics of earthquakes

PGA (cm/s^2)	Shear wave velocity (m/s)	Epicentral distance (km)	Station
107.91	360–750	25	80053 Pasadena, CIT Athenaeum
317.844	360–750	24	24278 Castaic, Old Ridge Route
188.352	360–750	19.6	126 Lake Hughes #4
59.841	<750	60.7	290 Wrightwood, 6074 Park Dr
154.017	<750	23.5	127 Lake Hughes #9
19.62	180–360	86.6	111 Cedar Springs, Allen Ranch
206.01	180–360	21.2	135 LA, Hollywood Stor Lot
38.259	180–360	91	130 LB, Terminal Island
46.107	180–360	136	113 Colton, So Cal Edison
26.487	180–360	63	12331 Hemet Fire Station
30.411	180–360	82	272 Port Hueneme

In the above equations for frequency of harmonic waves, i.e., ω, the potential functions are as follows:

$$\psi_{SV} = A_S \exp i\omega \left(\frac{\sin\theta_0}{\beta}x - \frac{\sin\theta_0}{\beta}z - t \right) \quad (6)$$

$$\varphi_{SP} = A_{SP} \exp i\omega \left(\frac{\sin\theta_1}{\alpha}x - \frac{\sin\theta_1}{\alpha}z - t \right) \quad (7)$$

$$\psi_{SS} = A_{SS} \exp i\omega \left(\frac{\sin\theta_0}{\beta}x - \frac{\sin\theta_0}{\beta}z - t \right) \quad (8)$$

where α and β are the propagation velocities of P and S waves, respectively. They can be expressed as follows (Datta 2010):

$$\alpha = \left[\frac{E(1-\nu)}{\rho(1+\nu)(1-2\nu)} \right]^{\frac{1}{2}} \quad (9)$$

$$\beta = \left[\frac{E}{2\rho(1+\nu)} \right]^{\frac{1}{2}} \quad (10)$$

where E, ρ, and ν are the Young's modulus, the mass density, and the Poisson ratio of the soil mass, respectively. The value of coefficients, α and β, depends on the soil properties; at the surface of the earth, their values vary in the range of 5 to 7 km s^{-1} and 3 to 4 km s^{-1}, respectively (Datta 2010). According to Fig. 1, the angle of incidence (θ_0) and the angle of reflection of SV waves (θ_2) are equal. The angle of reflected P wave is denoted as θ_1. By imposing the free shear stress condition at the ground surface:

$$\tau_{xz}|_{z=0} = \frac{\partial w}{\partial x} + \frac{\partial w}{\partial z}\bigg|_{z=0} = 0 \quad (11)$$

The rocking component can be obtained from Eqs. 3 to 11 as follows:

$$\varphi_{gy} = \frac{\partial w}{\partial x} = \frac{\partial^2 \varphi_{SP}}{\partial z \partial x} - \frac{\partial^2 (\psi_{SV} + \psi_{SS})}{\partial x^2}$$
$$= (i\omega)^2 \frac{\cos\theta_1}{\alpha} \cdot \frac{\sin\theta_1}{\alpha}\varphi_{SP} - \left[\left(i\omega\frac{\sin\theta_0}{\beta} \right)\psi_{SV} + \left(i\omega\frac{\sin\theta_0}{\beta} \right)^2 \psi_{SS} \right] \quad (12)$$

According to the Snell law, $\sin\theta_0/\beta = \sin\theta_1/\alpha$, Eq. (13) can be obtained:

$$\varphi_{gy} = \frac{i\omega}{C_x} = e^{\frac{\pi}{2}i}\left(\frac{\omega}{C_x}R_w e^{i\theta_w} \right) = \left(\frac{\omega}{C_x}R_w \right)\left(e^{\left(\frac{\pi}{2}+\theta_w\right)i} \right) \quad (13)$$

Table 2 NEHRP Site Classification, FEMA 450-1/2003 Edition

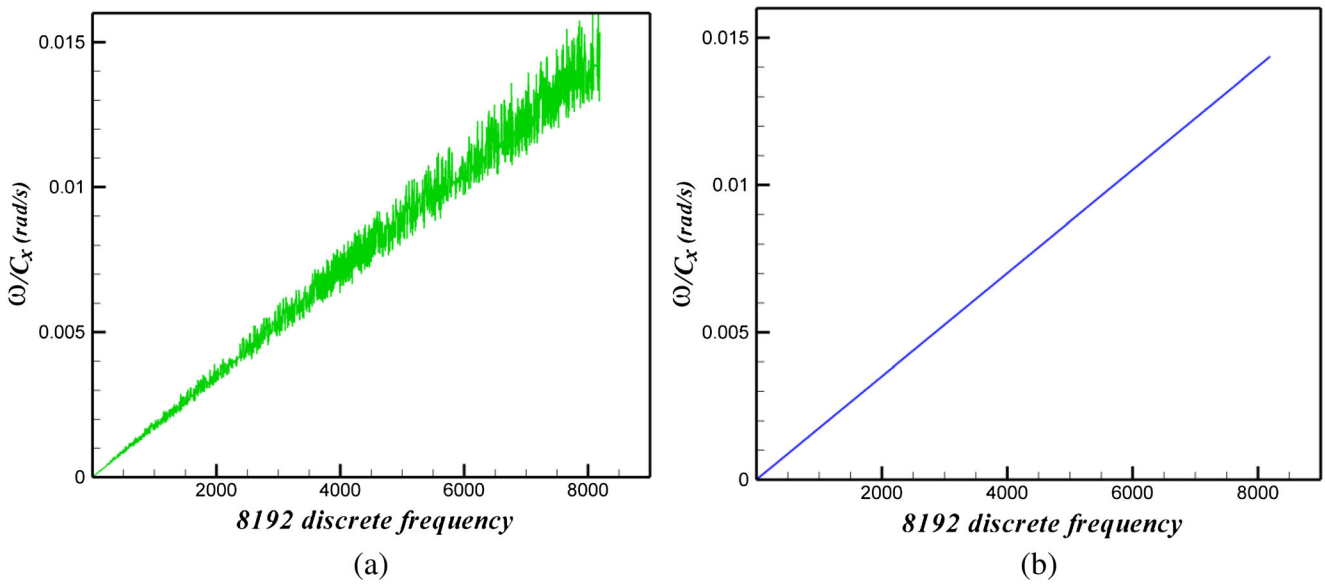| Site class	Description	Average shear wave velocities (m/s)
A	Hard rock	≥1,500
B	Rock	760 to 1,500
C	Very dense soil and soft rock	360 to 760
D	Stiff soil	180 to 360
E	Soft clay soil	≤180

Fig. 2 The ratio of ω/C_x. **a** Frequency dependent. **b** Frequency independent

In which $C_x = \beta/\sin\theta_0$, R_w, and θ_W are translational component and its phase. These equations can also be applied for the other rocking component φ_{gx}.
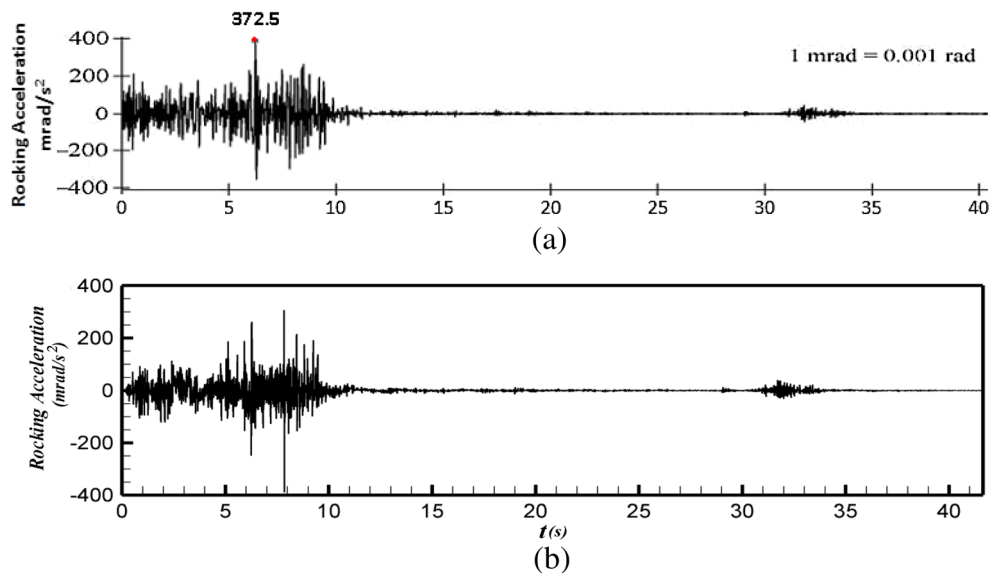
Incidence SH waves

According to Fig. 1b, there is no mode conversion in the case of incident SH wave; hence, there is only one reflected SH wave with $\theta_2 = \theta_0$ and $A_2 = A_0$. The potential functions of incident and reflected waves are as follows:

$$V_{SH} = A_0 \exp i\omega \left(\frac{\sin\theta_0}{\beta}x - \frac{\cos\theta_0}{\beta}z - t \right) \tag{14}$$

$$V_{SH'} = A_1 \exp i\omega \left(\frac{\sin\theta_0}{\beta}x - \frac{\cos\theta_0}{\beta}z - t \right) \tag{15}$$

Displacement field v, which is caused by the incident and reflected waves in y direction, is as follows:

$$v = 2V_{SH} = 2A_0 \exp i\omega \left(\frac{\sin\theta_0}{\beta}x - t \right) \tag{16}$$

Fig. 3 Rocking component acceleration for San Fernando earthquake by **a** Lee and Liang (2008) and **b** in this research

135 LA - Hollywood Stor Lot

80053 Pasadena - CIT Athenaeum

24278 Castaic - Old Ridge Route

127 Lake Hughes #9
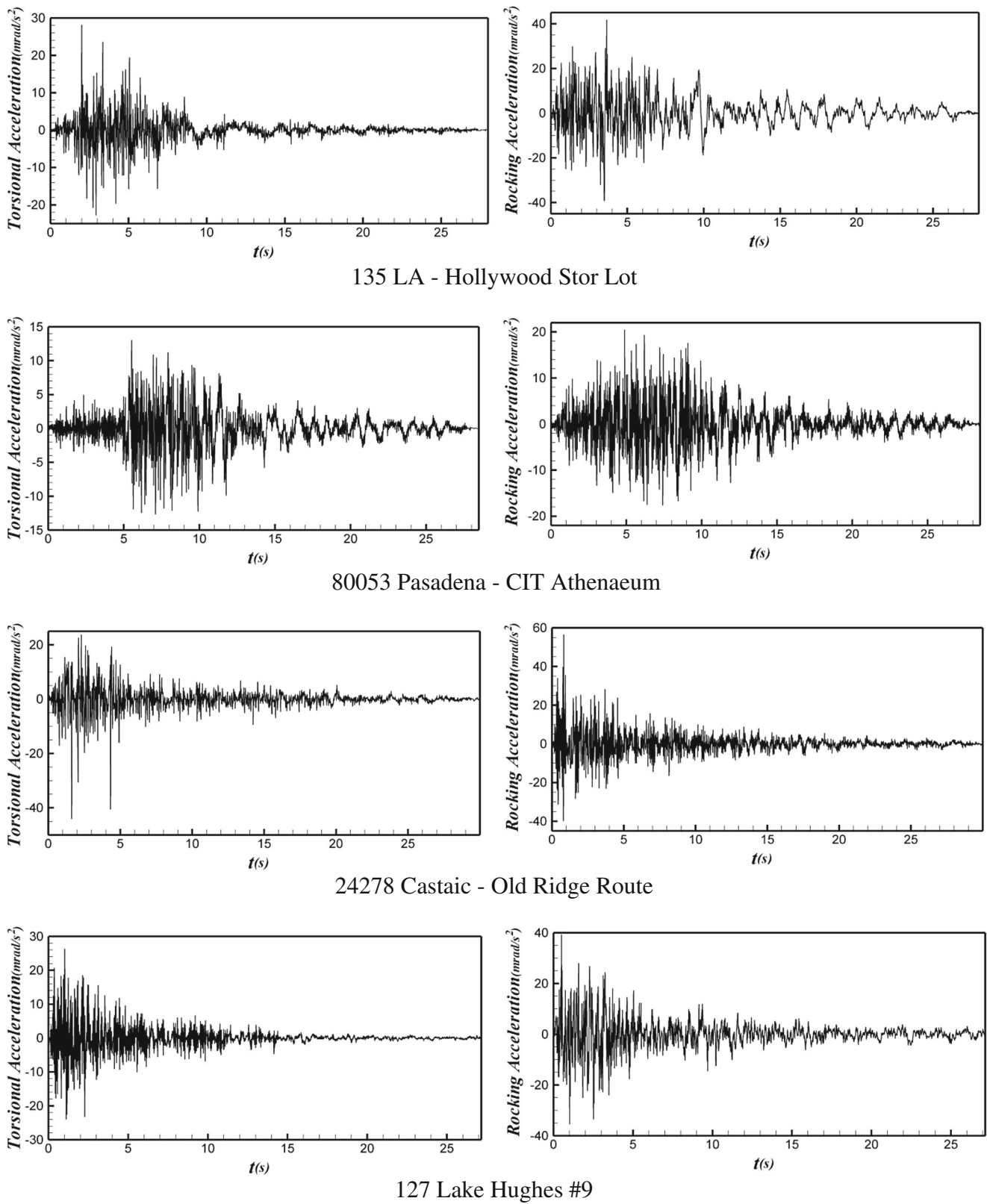
Fig. 4 Time history of rocking and torsional components for near-fault earthquake

Since u does not depend on the out-of-plane coordinate, the consideration of Eqs. (13)–(16) leads to the torsional component, φ_{gz}:

$$\varphi_{gz} = \frac{1}{2}\left(\frac{-\partial u}{\partial y} - \frac{\partial v}{\partial x}\right) = \frac{1}{2}\frac{\partial v}{\partial x}\bigg|_{Z=0} = \frac{\partial V_{SH}}{\partial x} = i\omega\frac{\sin\theta_0}{\beta}\frac{v}{2} = \frac{i\omega}{2C_x}v$$

$$\Rightarrow \varphi_{gz} = e^{\frac{\pi}{2}i}\left(\frac{\omega}{2C_x}R_v e^{i\theta_v}\right) = \left(\frac{\omega}{2C_x}R_v\right)\left(e^{\left(\frac{\pi}{2}+\theta_v\right)i}\right)$$

(17)

In which $C_x = \beta/\sin\theta_0$, R_v, and θ_v are translational component and its phase. It is assumed that the translational components u, v, and w of the ground motion at the free surface are available through measurements. Equations (13) and (17) could be used to define the rocking and torsional components of ground motion, respectively. These equations show that the amplitude of rotational components is related to translational component amplitude, $(R_w.\omega/C_x)$ or $(R_v.\omega/2C_x)$, and their phase difference is $\pi/2$. However, this is not feasible with the state-of-the-art seismology yet. Therefore, in order to apply these equations to define φ_{gy} and φ_{gz}, the value of incident angle θ_0 should be identified. How to determine unknown parameters is the subject of the following development.

Incidence angle of SV and SH waves

A modification of a developed approach by Li et al. (2004) was used to calculate the angle of incident waves. Using this approach while introducing ($x = \sin\theta_0$) as well as considering Snell's law, Eqs. (16) and (17) were employed to obtain the angle of incident SV and SH waves.

$$G = \frac{2x\sqrt{1-K^2x^2}}{K(1-2x^2)}, \quad \theta_0 < \theta_c$$

(18)

$$G = -\frac{2x\sqrt{1-K^2x^2}}{iK(1-2x^2)}, \quad \theta_0 > \theta_c$$

(19)

where $G = \tan\overline{e} = w/u$ and $G = \tan\overline{e} = w/v$ are related to rocking component in x–z and y–z plane due to SV waves, respectively; $G = \tan\overline{e} = v/u$ is related to torsional component in x–y plane due to SH waves; $K = \alpha/\beta$ and $\theta = \arcsin(\alpha/\beta)$ are the incident critical angle.

Result and discussion

In this paper, 11 earthquakes are selected to study their relative rotational components. Characteristics of these 11 earthquakes are listed in Table 1.

The effects of soil type were considered in producing rocking and torsional acceleration components of earthquakes

**Fig. 5** Time history of rocking and torsional components for fare-fault earthquake ▶

on the basis of transitional components using Eqs. (13) and (17); it was feasible by studying a wide range of average shear wave velocities from about 200 to 2,000 m/s in top 30 m of soil layers in three soil types A, C, and D (mostly close to E). As shown in Table 2, specifications of these soil types were determined in accordance with National Earthquake Hazards Reduction Program (NEHRP) Site Classification.

In this research, the wave velocity is considered frequency dependent as shown in Fig. 2. For San Fernando earthquake, the time history of rocking component obtained by Lee and Liang (2008) and this research is also shown in the figure.

For verification of improved approach in this research, our results are compared with the results of Lee and Liang (2008). In the mentioned work, the San Fernando earthquake is considered for calculation. This earthquake is recorded on February 9, 1971 at Pacoma dam station where its horizontal (S74W) and vertical components had a peak acceleration of 1,055 and 696 cm/s², respectively. The peak values of rocking and torsional accelerations are obtained (0.3725 and −0.2480 rad/s²) by Lee and Liang (2008) and (−0.3833 and −0.2545 rad/s²) by our research, respectively. The differences between these results are about 3 % that are due to different wave velocity and empirical scaling. For the San Fernando earthquake, the time history of rocking component obtained by Lee and Liang (2008) and this research is also shown in Fig. 3.

Torsional and rocking time histories for the near-fault and far-fault earthquake are shown in Figs. 4 and 5, respectively. As it can be seen in the figures, peak rotational acceleration for near-fault earthquakes is more than far-fault earthquakes. That is why, after passing distances because of reduction as a result of wave pass in its way, the intensity of the waves reduces. Attenuation relationship is usually a function of the magnitude of the earthquake and the distance from the source. Comparison of near-fault and far-fault earthquake records also indicates that near-fault ground motions often exhibit distinguishable pulse-like features in their acceleration time histories. Pulses which occur at the beginning of the record indicate a significant energy release in a short time. The pulse contents in acceleration time histories have also been found important for structural responses. This feature is one of the most important characteristics of near-fault ground motions. The figures also indicate that the peak rocking acceleration is more than the peak torsional acceleration.

Due to problems in measurement of rotational components, we tried to establish a specific relationship between translational, torsional, and rocking component (Ghayamghamian and Nouri 2007; Suryanto et al. 2006a, b). In this part, the relation between peak torsional acceleration (PTA) and peak rocking acceleration and peak of translational acceleration of
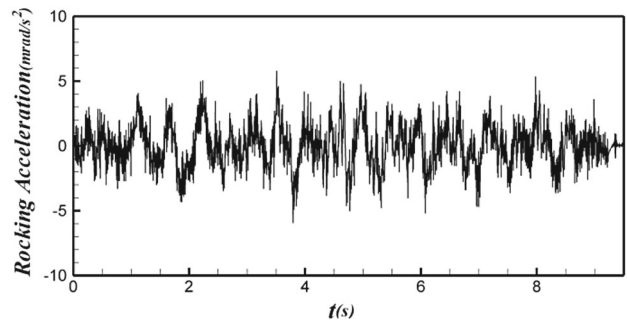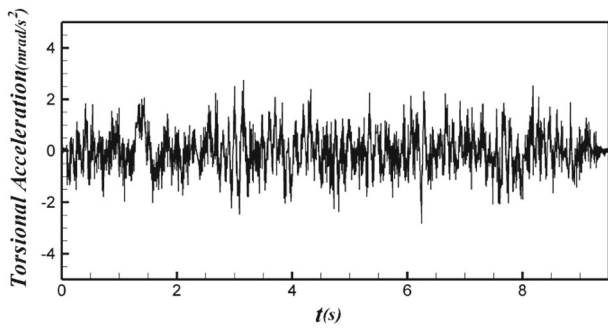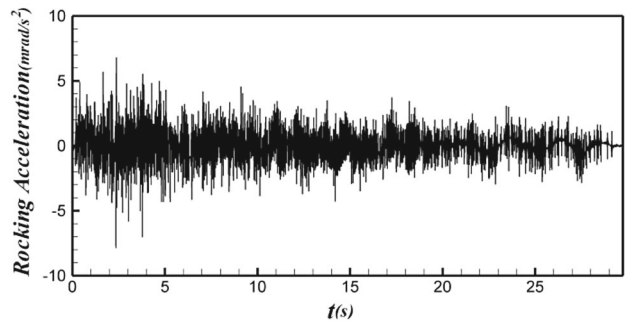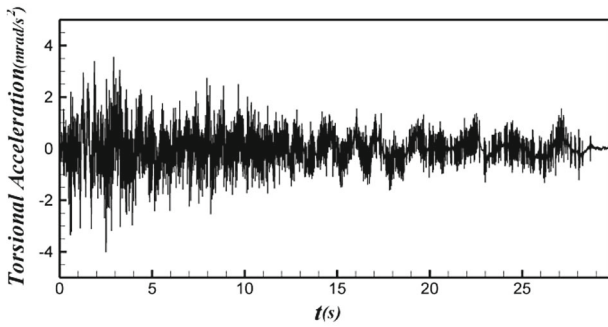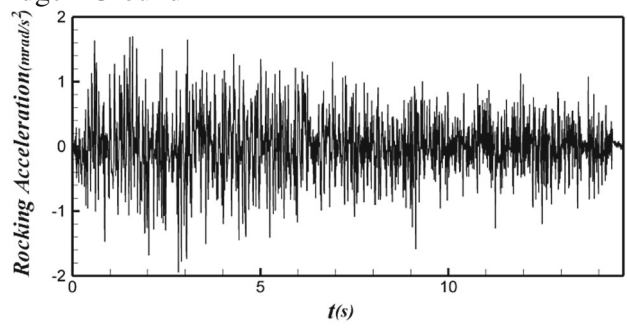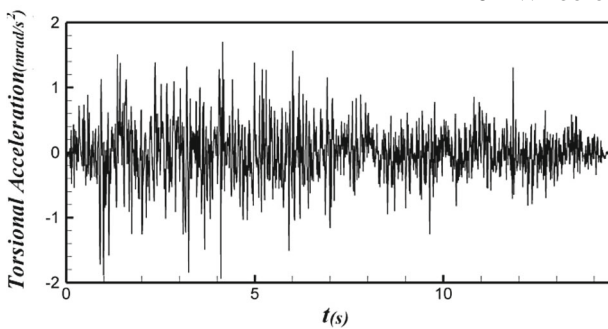
113 Colton - So Cal Edison
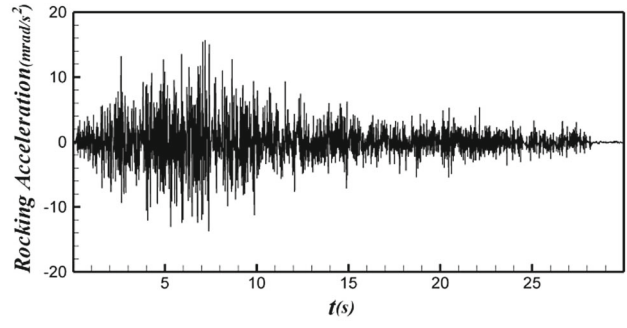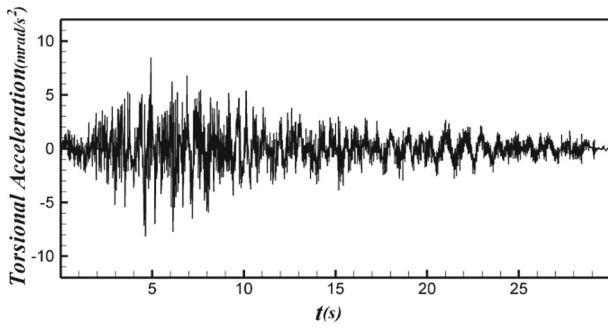
12331 Hemet Fire Station
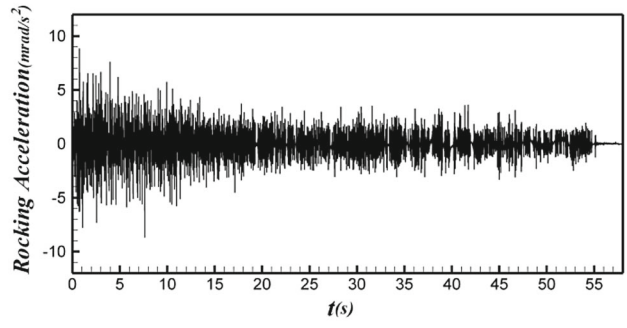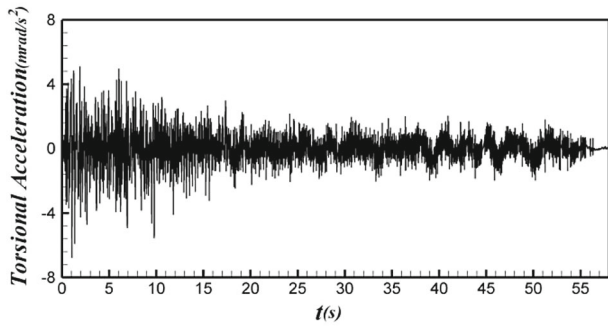
272 Port Hueneme

1102 Wheeler Ridge - Ground

111 Cedar Springs, Allen Ranch

(PGA) and also the relation between peak rocking acceleration (PRA) and peak rocking acceleration have been investigated. As can be seen in Fig. 6a, b with the increase of peak translational acceleration, the peak rocking and torsional accelerations increase. In earthquakes with low peak translational acceleration, these changes are so small. The peak values of translational and rocking accelerations increase significantly with the increase of translation acceleration. In addition, Fig. 3 shows that the relation between peak translational acceleration and peak rocking and torsional accelerations and relation between peak rocking acceleration and peak torsional

acceleration is precisely linear. Correlation coefficient (R^2) close to 1 indicates that values from relations are close to available data.
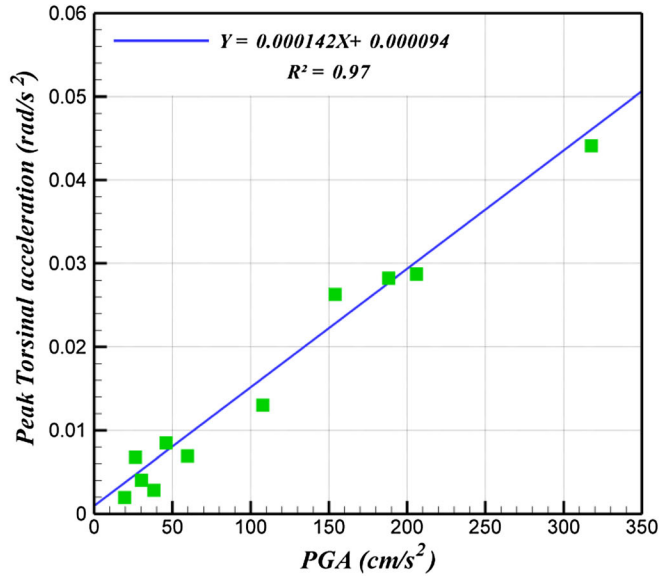
$$PRA = 0.0020\ PGA + 0.00237 \tag{20}$$

$$PTA = 0.000142\ PGA + 0.000094 \tag{21}$$

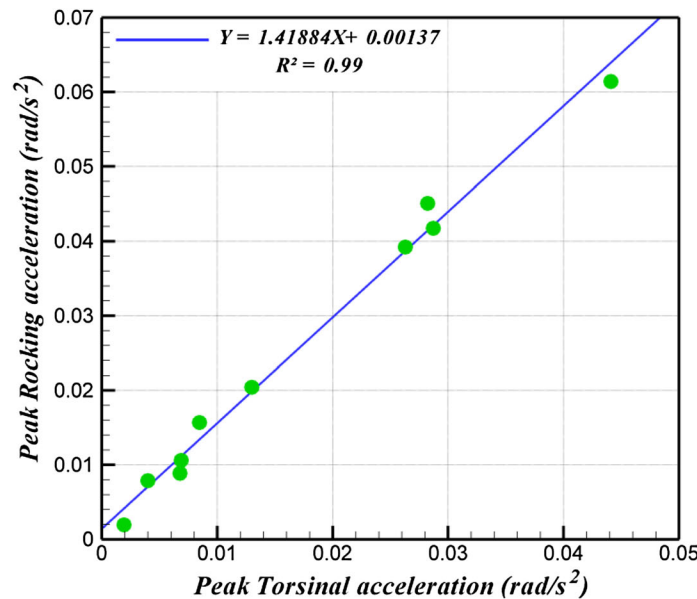$$PRA = 1.41884\ PTA + 0.00137 \tag{22}$$
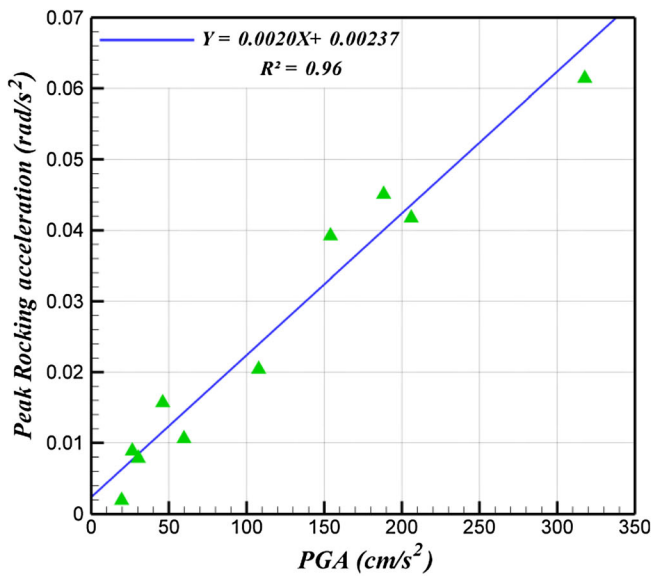
Fig. 6 a Relation between peak rocking acceleration and peak torsional acceleration. b Relation between peak torsional acceleration and peak torsional acceleration. c Relation between peak rocking acceleration and peak torsional acceleration
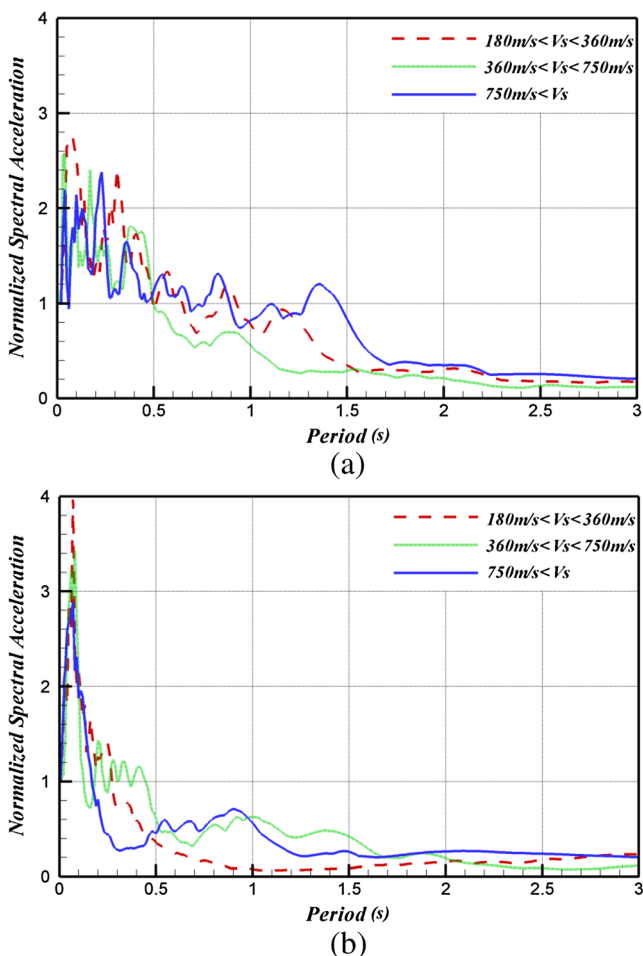
Fig. 7 Effect of the near-fault and far-fault earthquakes and soil shear wave velocity on the normalized response spectra of the rocking component. **a** Far-fault. **b** Near-fault

Fig. 8 Effect of the near-fault and far-fault earthquakes and soil shear wave velocity on the normalized response spectra of the torsional component. **a** Far-fault. **b** Near-fault

Equation 22 shows that the peak rocking acceleration is higher than the peak torsional acceleration. In this study, the ratio between the peak rocking acceleration and the peak torsional acceleration is 1.41884.

Figure 7 shows the effect of the near-fault and far-fault earthquakes and soil shear wave velocity on the normalized response spectra of the rocking component. By comparing the spectra of the near and far field of faulting, it is observed that the values of the normalized response spectra for almost every type of soil have a maximum value greater than its corresponding far field. According to the results of the inelastic design spectrum, in near field, rocking components for periods of less than 1 s rather than periods over 1 s and in far field for periods of less than 2 s compared to periods greater than 2 s contain considerable quantities. It shows that for far-field earthquakes, low period structures are significantly influenced by rocking components, and for near-field earthquakes, long period structures are significantly influenced by rocking components. Generally, the values of normalized response spectra reduce by an increase in shear wave velocity. But if site fundamental period is equal to rocking component period, amplification takes place
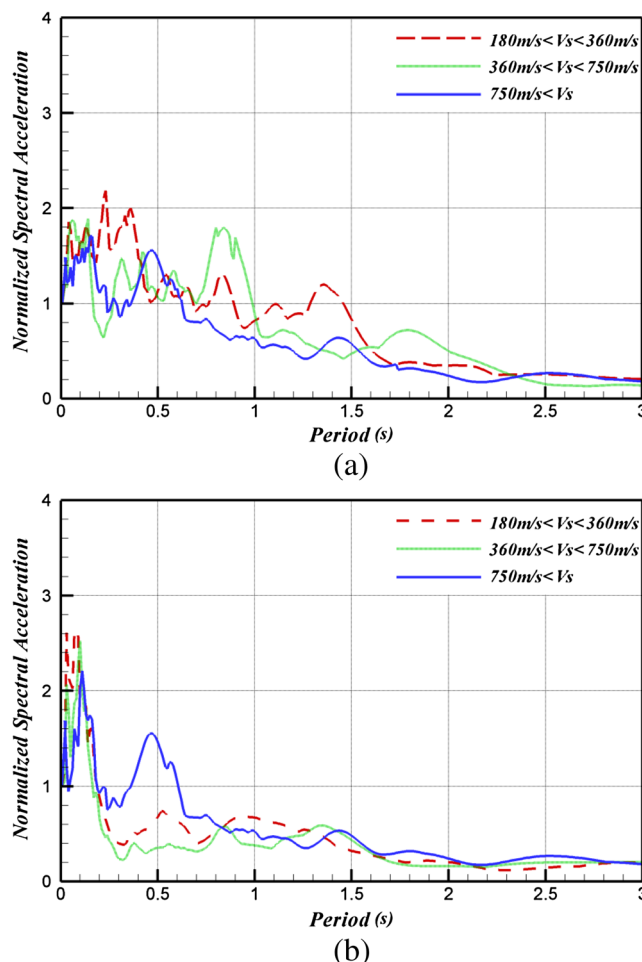
and the values of the normalized response spectra for soft sites have higher amounts than hard sites.

Figure 8 shows the effect of the near-fault and far-fault earthquakes and soil shear wave velocity on the normalized response spectra of the torsional component. As can be seen in the figure, the values of torsional normalized response spectra in near field for periods of less than 0.6 s compared to periods greater than 0.7 s and in far field for periods of less than 1.5 s rather than periods longer than 1.5 s are far more. This indicates that torsional components are more important at low periods.

By comparing Figs. 7 and 8, it is observed that the values of the normalized response spectra at low periods (less than 1 s, the period of the conventional buildings) have higher amounts than at high periods. This is indicates that rotational components are more important at low periods. This behavior can be explained with the fact that the rotational components have a direct relation with derivation of one higher order of translational components, so rocking and torsional components have a more frequency content in comparison with similar horizontal components in high frequencies, and this difference in

frequency content causes rotational components to become more important in loading structure with low periods.

Conclusions

Rotational components can significantly affect the behavior of structures and consequently may have structural damage and failure. Due to the high cost of rotational ground motion components recorded by the equipments which have not been developed adequately, the use of transitional components of the ground motion for generation rotational components is one of the most widely used methods. In this study, the rotational component of production technique was described, and the influences of soil type and distance from the fault on the rotational component were investigated. The results are summarized as follows:

1. The value of the normalized response spectra for soft soil is more than stiff soil, but for far-fault earthquake, it is less than near-fault earthquake.
2. The rotational components showed a direct relation with a higher order derivation of translational components, therefore, more frequency content. As a consequence, the torsional components are more important at low periods.
3. It was that the relation between peak acceleration values of torsional and rocking components and peak acceleration value of translational component and also the relation between peak acceleration values of rocking components and peak acceleration value torsional component acceleration are linear.
4. When seismic waves were propagated in the stiff soils at the same conditions between two earthquake components (i.e., in equal peak ground acceleration in vertical and horizontal direction), the shear wave velocity in the stiff soil will be higher than the soft soils; hence, lower peak acceleration was achieved in the rotational components compared to propagation in the soft soil.

References

Abbaszadeh Shahri A, Esfandiyari B, Hamzeloo H (2011) Evaluation of a nonlinear seismic geotechnical site response analysis method subjected to earthquake vibrations (case study: Kerman Province, Iran). Arab J Geosci 4:1103–1116

Ashtiany GM, Singh MP (1986) Structural response for six correlated earthquake components. Earthq En Struct D 14:103–119

Bararnia H, Ghasemi E, Soleimani S, Ghotbi A, Ganji DD (2012) Solution of the Falkner–Skan wedge flow by HPM–Pade method. Adv Eng Softw 43:44–52

Bouchon M, Aki K (1982) Strain, tilt and rotation associated with strong ground motion in the vicinity of earthquake faults. Bull Seism Soc Am 72:1717–1738

Bycroft GN (1980) Soil-foundation interaction and differential ground motions. Earthq En Struct D 8:397–404

Castellani A, Boffi G (1989) On the rotational components of seismic motion. Earthq En Struct D 18:785–797

Chattopadhyay G, Chattopadhyay S (2009) Dealing with the complexity of earthquake using neurocomputing techniques and estimating its magnitudes with some low correlated predictors. Arab J Geosci 2: 247–255

Choobbasti AJ, Tavakoli H, Kutanaei SS (2014) Modeling and optimization of a trench layer location around a pipeline using artificial neural networks and particle swarm optimization algorithm. Tunn Undergr Space Technol 40:192–202

Datta TK (2010) Seismic analysis of structures. John Wiley and Sons

De La Llera JC, Chopra AK (1994) Accidental torsion in buildings due to base rotational excitation. Earthq En Struct D 23:1003–1021

Deif A, El-Hussain I, Al-Jabri K, Toksoz N, El-Hady S, Al-Hashmi S, Al-Toubi K, Al-Shijbi Y, Al-Saifi M (2013) Deterministic seismic hazard assessment for Sultanate of Oman. Arab J Geosci 6:4947–4960

El-Hussain I, Deif A, Al-Jabri K, Mohamed AME, Al-Habsi Z (2013) Efficiency of horizontal-to-vertical spectral ratio (HVSR) in defining the fundamental frequency in Muscat Region, Sultanate of Oman: a comparative study. Arab J Geosci. doi:10.1007/s12517-013-0948-8

Ganji DD, Bararnia H, Soleimani S, Ghasemi E (2009) Analytical solution of the magneto-hydrodynamic flow over a nonlinear stretching sheet. Mod Phy Lett B 23:2541–2556

Ghayamghamian MR, Nouri GR (2007) On the characteristics of ground motion rotational components using Chiba dense array data. Earthq En Struct D 36:1407–1429

Ghayamghamian MR, Nouri GR, Igel H, Tobita T (2009) Measuring the effect of torsional ground motion on structural response-code recommendation for accidental eccentricity. Bull Seism Soc Am 99:1261–1270

Gomberg J (1997) Dynamic deformations and M6.7, Northridge, California earthquake. Soil Dyn Earthq Eng 16:471–494

Gordon DW, Bennett TJ, Herrmann RB, Rogers AM (1970) The south-central Illinois earthquake of November 9, 1968: macroseismic studies. Bull Seism Soc Am 60:953–971

Graizer VM (2009) Tutorial on measuring rotations using multipendulum systems. Bull Seismol Soc Am 99:1064–1072

Hart GC, DiJulio RM, Lew M (1975) Torsional response of high-rise buildings. ASCE J Struct Division 101:397–415

Huang BS (2003) Ground rotational motions of the 1999 Chi Chi, Taiwan earthquake as inferred from dense array observations. Geophys Res Lett 30:1307–1310

Igel H, Schreiber U, Flaws A, Schuberth B, Velikoseltsev A, Cochard A (2005) Rotational motions induced by the M8.1 Tokachi-Oki earthquake, September 25, 2003. Geophys Res Lett 32:L08309

Igel H, Cochard A, Wassermann G, Schreiber U, Velikoseltsev A, Pham Dinh N (2007) Broadband observations of rotational ground motions. Geophys J Int 168:182–197

Jalaal M, Nejad MG, Jalili P, Esmaeilpour M, Bararnia H, Ghasemi E, Soleimani S, Ganji DD, Moghimi SM (2011) Homotopy perturbation method for motion of a spherical solid particle in plane couette fluid flow. Comput Math Appl 16:2267–2270

Janalizadeh A, Kutanaei SS, Ghasemi E (2013) Control volume finite element modeling of free convection inside an inclined porous enclosure with a sinusoidal hot wall. Scientia Iranica A 20(5): 1401–1414

Kalanisarokolayi L, Navayineya B, Hosainalibegi M, Vaseghi AJ (2008) Dynamic analysis of water tanks with interaction between fluid and structure. 14th WCEE, Beijing, China

KalaniSarokolayi L, NavayiNeya B, Tavakoli HR (2012) Rotational components generation of earthquake ground motion using translational components. 15th WCEE, Lisbon

Kutanaei SS, Ghasemi E, Bayat M (2011) Mesh-free modeling of two-dimensional heat conduction between eccentric circular cylinders. Int J Phys Sci 6(16):4044–4052

Kutanaei SS, Roshan N, Vosoughi A, Saghafi S, Barar B, Soleimani S (2012) Numerical solution of stokes flow in a circular cavity using mesh-free local RBFDQ. Eng Anal Boundary Elem 36(5):633–638

Lee VW, Liang L (2008) Rotational components of strong motion earthquakes. 14th WCEE Beijing, China

Lee VW, Trifunac MD (1985) Torsional accelerograms. Soil Dyn Earthquake Eng 6:75–89

Lee VW, Trifunac MD (1987) Rocking strong earthquake accelerations. Soil Dyn Earthquake Eng 6:75–89

Li HN, Sun LY, Wang SU (2004) Improved approach for obtaining rotational components of seismic motion. Nuclear Eng and Design 232:131–137

Liu CC, Huang BS, Lee W, Lin CJ (2009) Observation rotational and translational ground motion at the HGSD station in Taiwan from 2007 to 2008. Bull Seism Soc Am 99:1228–1236

MirMohammad Hosseini SM, Asadollahi Pajouh M (2012) Comparative study on the equivalent linear and the fully nonlinear site response analysis approaches. Arab J Geosci 5:587–597

Newmark NM (1969) Torsion in symmetrical buildings, Proc. World Conf. Earthquake Engineering, 4th, Santiago, Chile 2, A-3

Niazi M (1986) Inferred displacements, velocities and rotations of a long rigid foundation located at El Centro differential array site during the 1979 Imperial Valley, California, earthquake. Earthq En Struct D 14:531–542

Nigbor RL (1994) Six degree-of-freedom ground-motion measurement. Bull Seismol Soc Am 84:1665–1669

Nouri GR, Ghayamghamian MR, Hashemifard M (2010) A comparison among different methods in the evolution of torsional ground motion. J Iran Geophys 4:32–44

Politopoulos I (2010) Response of seismically isolated structures to rocking-type excitations. Earthq En Struct D 39:325–342

Rafi Z, Ahmed N, Ur-Rehman S, Azeem T, Abd el-aal AK (2013) Analysis of Quetta-Ziarat earthquake of 29 October 2008 in Pakistan. Arab J Geosci 6:1731–1737

Rezaei S, Choobbasti AJ, Kutanaei SS (2013) Site effect assessment using microtremor measurement, equivalent linear method, and artificial neural network (case study: Babol, Iran). Arab J Geosci. doi:10.1007/s12517-013-1201-1

Shahri AA, Esfandiyari B, Hamzeloo H (2011) Evaluation of a nonlinear seismic geotechnical site response analysis method subjected to earthquake vibrations (case study: Kerman Province, Iran). Arab J Geosci 4:1103–1116

Soleimani S, Ganji DD, Gorji M, Bararnia H, Ghasemi E (2011) Optimal location of a pair heat source-sink in an enclosed square cavity with natural convection through PSO algorithm. Int Commun Heat Mass Transf 38:652–658

Soleimani S, Sheikholeslami M, Ganji DD, Gorji M (2012) Natural convection heat transfer in a nanofluid filled semi-annulus enclosure. Int Commun Heat Mass Transf 39:565–574

Spudich P, Steck LK, Hellweg M, Fletcher JB, Baker LM (1995) Transient stresses at Parkfield, California, produced by the M 7.4 Landers earthquake of June 28, 1992: observations from the UPSAR dense seismograph array. J Geophys Res 100:675–690

Stedman GE, Li Z, Bilger HR (1995) Sideband analysis and seismic detection in large ring laser. Appl Opt 5375–5385

Suryanto W, Igel H, Wassermann J, Cochard A, Schuberth B, Vollmer D, Scherbaum F, Schreiber U, Velikoseltsev A (2006a) First comparison of array-derived rotational ground motions with direct ring laser measurements. Bull Seism Soc Am 96:2059–2071

Suryanto W, Igel H, Wassermann J, Cochard A, Schuberth B, Vollmer D, Scherbaum F, Schreiber U, Velikoseltsev A (2006b) First comparison of array-direct ring laser measurements. Bull Seismol Soc Am 96:2059–2071

Taeibi-Rahni M, Ramezanizadeh M, Ganji DD, Darvan A, Ghasemi E, Soleimani S, Bararni H (2011) Comparative study of large eddy simulation of film cooling using a dynamic global-coefficient subgrid scale eddy-viscosity model with RANS and Smagorinsky modeling. Int Commun Heat Mass Transf 38:659–667

Takeo M (1998) Ground rotational motions recorded in near-source region of earthquakes. Geophys Res Lett 25:789–792

Takeo M (2009) Rotational motions observed during an earthquake swarm in April 1998 offshore Ito, Japan. Bull Seismol Soc Am 99:1457–1467

Tavakoli H, Omran OL, Kutanaei SS, Shiade MS (2014) Prediction of energy absorption capability in fiber reinforced self-compacting concrete containing nano-silica particles using artificial neural network. Latin Am J Solids Struct 11(6):966–979

Wolf JP, Obernhueber P, Weber B (1983) Response of a nuclear plant on a seismic bearings to horizontally propagating waves. Earthq En Struct D 11:483–499

Zembaty Z, Boffi G (1994) Effect of rotational seismic ground motion on dynamic response of slender towers. Eur Earthq En 8:3–11